

A Navigational Framework Combining Visual Servoing and Spiral Obstacle Avoidance Techniques

Marcus Futterlieb^{1,2}, Viviane Cadenat^{1,2} and Thierry Sentenac¹

¹CNRS, LAAS, 7 avenue du Colonel Roche, F-31400 Toulouse, France

²Univ de Toulouse, UPS, LAAS, F-31400 Toulouse, France

Keywords: Navigation, Control, Mobile Robotics, Visual Servoing, Navigational Framework, Obstacle Avoidance.

Abstract: This paper presents a navigational framework which enables a robot to perform Long Range Navigation in the context of the Air-Cobot-Project in which a robot is used to execute an autonomous pre-flight inspection on an aircraft. The robot is equipped with Laser range finders and a mobile stereo camera system. The idea is to guide the robot to the pre-defined checkpoints using a Visual Servoing controller based on video data, while avoiding static and moving obstacles. The contribution of the paper is an avoidance technique derived from the spiral flight path of insects applied to the Laser range data. Simulation results validate the whole approach.

1 INTRODUCTION

In mobile robotics, especially for industrial robots, it is very important to have a robust and reliable navigation strategy to guide the robot through its workplace. With human workforce in its vicinity it is necessary to keep the robot in a caged environment or alternatively equip it with some sort of obstacle avoidance (OA). The objective of Air-Cobot-Project is to design, develop and evaluate a robot able to assist or solely inspect an aircraft before takeoff and provide diagnosis. Therefore, the robot has to move autonomously between different checkpoints while taking into account the presence of both men and vehicles in its vicinity. It also must be collaborative with the airport information systems.

Thus, the robot has to perform a long range navigation assignment which involves several tasks respectively related to perception, environment modeling, localization, path planning and supervision which will be coupled within a navigational framework. In the project, the perception task is based on both cameras and laser sensors. A modeling task provides the metric and the topologic maps describing the airport environment with the different checkpoints to be reached successively. Path planning has to compute a path allowing the robot to reach the aircraft inspection site starting from its initial position. Furthermore, the localization method has to provide the pose of the robot relatively to the aircraft and to a global fixed frame. The robot's motion will be determined by a

supervisor, a high level controller, which will choose the most appropriate controller depending on the context. In our case, several controllers will be available: a trajectory following controller allowing to reach the inspection site; a Visual Servoing (VS) controller allowing to reach each checkpoint thanks from visual data of the aircraft taken by the embedded cameras; an OA controller ensuring collision free execution of the task.

Our contribution is related to visual navigation in possibly cluttered environment, meaning that a camera is used as the main sensor to move the robot towards the goal. To do so we can use either global or local approaches. Generally speaking, global methods assume that the robot is provided a map prior to the navigation. With the help of this map long range displacements are conceivable. However, as this map can only take into account obstacles which are known a priori it must be updated whenever new objects arise. These techniques appear to introduce some rigidity in the navigation system even if improvements have been made by developing methods allowing to re-plan a new path (Koenig and Likhachev, 2005) (Lamiriaux et al., 2004) or to locally modify the robot's trajectory (Owen and Montano, 2005) (Damas and Santos-Victor, 2009).

On the contrary, local methods do not require a map, meaning that obstacles do not need to be known a priori but can be detected during the mission. Furthermore, the robot will move through the scene depending on the goal to be reached and on the sen-

sory data perceived during the navigation. Some well known techniques such as potential field (Khatib and Chatila, 1995) or the VFH* (Ulrich and Borenstein, 2000) technique belong to this category. More recent works have proposed to couple two controllers allowing to reach the goal and to guarantee non-collision (Folio and Cadenat, 2005) (Vilca et al., 2013). These methods tend to be more reactive, but they can suffer from local minima and only allow for short range displacements.

Therefore, it seems interesting to couple a global with a local approach to take advantage of both methods. This is a concept presented in (Matsumoto et al., 1996) and which has been re-used in (Cherubini et al., 2013), (Cherubini et al., 2012) and (Adrien D. Petiteville and Cadenat, 2012). To summarize, the approach consists in defining the path to be followed in a sequence of images known as visual road. Making the robot follow this path is achieved with the help of a VS controller. OA can be performed by coupling a proper controller to the VS.

In this article we will focus on the design of a new OA controller in the background of (Adrien D. Petiteville and Cadenat, 2012). For the context of our project, the robot has to mainly avoid unexpected static and moving obstacles. It is inspired by an article showing that insects perform a spiral path around a light source (Boyadzhiev, 1999). Following a reasoning similar to the one developed in (Mcfadyen et al., 2012b), (Mcfadyen et al., 2012a) our idea is to adapt this method to make a robot avoid the obstacle by performing a spiral around a specific point to be defined. We will provide some guidelines about the choice of this point and the avoidance control law.

The structure of this article will be the following: In the next section, we will introduce the necessary conceptual basics of our work. After that we present our first theoretical and simulation results about the obstacle avoidance method and give some results we have achieved through simulation with the Robot Operating System and Gazebo. Finally we provide a conclusion.

2 BACKGROUND ON VISUAL SERVOING AND ROBOT MODELING

2.1 Description of the Sensors and Robot

The robot we consider in this project is outfitted with numerous sensors dedicated to both, Non-destructive

Testing and navigation. In this article we will focus on the latter one. For navigational purposes, our robot is equipped with an IMU, a stereo camera system mounted on a pan tilt unit (PTU) and a laser range finder (LRF).

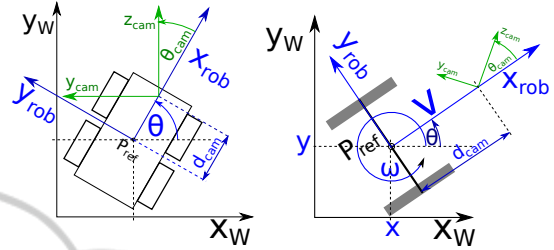


Figure 1: Real Life Robot Model (left) vs Robot Reference Kinematic Model(right).

2.2 Kinematic Model of the Robot

Let us consider Figure 1. The robot's pose is defined by vector (x, y, θ) where (x, y) and θ are respectively its position and its orientation wrt the world frame $F_w(O, \vec{x}_w, \vec{y}_w, \vec{z}_w)$. Furthermore, we propose another frame $F_{rob}(P_{ref}, \vec{x}_{rob}, \vec{y}_{rob}, \vec{z}_{rob})$ attached to the robot and yet a final frame $F_{cam}(C, \vec{x}_{cam}, \vec{y}_{cam}, \vec{z}_{cam})$ attached to the camera system. The angle between F_{cam} and F_w is θ_{cam} and for this paper we will ignore the tilt degree of freedom of the system. We consider a non-holonomic 4-wheel skid-steering robot. Following (Campion et al., 1996), provided that point P_{ref} is chosen as a point on an imaginary axis that lies in between both wheel axis, its kinematic model is given by the following relations:

$$\begin{bmatrix} \dot{x}(t) \\ \dot{y}(t) \\ \dot{\theta}(t) \\ \dot{\theta}_{cam} \end{bmatrix} = \begin{bmatrix} \cos(\theta(t)) & 0 & 0 \\ \sin(\theta(t)) & 0 & 0 \\ 0 & 1 & 0 \\ 0 & 0 & 1 \end{bmatrix} * \begin{bmatrix} v(t) \\ \omega(t) \\ \omega_{cam}(t) \end{bmatrix} \quad (1)$$

where $\dot{q} = [v \ \omega \ \omega_{cam}]^T$ gathers the control inputs. While ω and ω_{cam} coincide with the angular velocities of the robot (about z_{rob}) and camera (about x_{cam}), v represents the linear velocity of the robot along its axis x_{rob} . From this result, we deduce the camera kinematic screw wrt F_w which is given by $T_c^{F_c}$ where J is the robot's Jacobian.

$$T_c^{F_c} = J\dot{q} \quad (2)$$

$$J = \begin{bmatrix} -\sin(\theta_{cam}) & d_{cam} * \cos(\theta_{cam}) & 0 \\ \cos(\theta_{cam}) & d_{cam} * \sin(\theta_{cam}) & 0 \\ 0 & -1 & -1 \end{bmatrix} \quad (3)$$

2.3 Visual Servoing

VS allows to control a robot using the information provided by a camera (Chaumette and Hutchinson, 2006). Roughly speaking, it can be divided into two main classes: 3D-VS, where the feature vector is presented in 3D and 2D-VS where the data used to control the robot is directly defined on visual cues. Since it is less sensitive to noise than 3D-VS, we have used the second kind of control. The goal is to make the current visual signals s converge to their reference values s^* obtained at the desired (for the camera) pose. To perform this task, we apply the VS technique given in (Chaumette and Hutchinson, 2006) to mobile robots as in (Pissard-Gibollet and Rives, 1995). The proposed approach relies on the task function formalism (Samson et al., 1991) and consists in expressing the VS-task by the following task function to be regulated to zero:

$$e_{VS} = s - s^* \quad (4)$$

In our case, the visual features s will be defined by a target made of a set of N points of coordinates (X_i, Y_i) in the image plane. By imposing an exponential decrease on e_{VS} , a controller making e_{VS} vanish is obtained in (Chaumette and Hutchinson, 2006):

$$\dot{q} = \begin{bmatrix} v \\ \omega \\ \omega_{cam} \end{bmatrix} = -\lambda * ((L * J)^{-1} * e_{VS}) \quad (5)$$

where λ is a positive scalar or a positive definite matrix and L represents the interaction matrix. This latter matrix allows to relate the variation of the visual features in the image to the camera kinematic screw. Hence it is crucial to compute \dot{q} . For one point L is given by the following expression:

$$L = \begin{bmatrix} 0 & \frac{X_i}{z_i} & X_i Y_i \\ -1 & \frac{Y_i}{z_i} & 1 + Y_i^2 \\ z_i & z_i & \end{bmatrix} \quad (6)$$

Here X_i and Y_i are the pixel coordinates in the camera frame and z_i represents the depth of this point i .

3 OBSTACLE AVOIDANCE

3.1 The Avoidance Strategy

As we have hinted in the introduction we strive to achieve obstacle avoidance with the help of spirals. In this paragraph, our work has been inspired by (Boydzhiev, 1999) where the author has shown that the

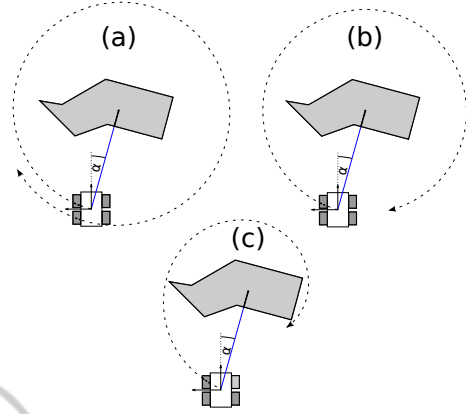


Figure 2: Three Schematics of Spiral Obstacle Avoidance Patterns.

flight path of insects around a light source results in a logarithmic spiral, also known as equiangular spiral. Figure 2 gives a general idea of how this concept can be applied for OA. Here we introduce three different options (an outward, a circle and an inward spiral trajectory) to circumvent a detected obstacle (gray polygon) using the spiraling concept by choosing α_d as described on page 4. Before we get into more detail on how to reach either a.), b.) or c.) let us take a step back and look on how we define certain parameters starting with the center point of the spiral.

3.2 Definition of the Spiral

3.2.1 Choosing the Spiral Center Point

To define the spiraling center point (SCP) we have chosen to use the data provided by the LRF. Of this data we will first define the obstacles face by searching for adjacent points. To make this following technique work, we have to assume that adjacent points belong to the same obstacle. Having detected the obstacle our next step is to define its boundaries. We will assume that the center point is located in between those boundaries and particularly in this paper we will consider that the SCP is in the middle of both outer boundaries of the obstacle. To choose the center of the obstacle we will now take the middle of both outer boundaries. Now we have the "heading" of the SCP, E_{center} (see blue line in Figure 3). What is still missing is the distance of this reference point towards the robot. Therefore, the algorithm will simply choose the shortest distance towards the obstacle from all LRF detected points (thickest red line). This distance will then be projected along the previously determined heading (blue line). To make sure that the points we have branded as the obstacles outer boundaries are valid and to avoid outliers, the border of

an obstacle must have adjacent points that are close enough to justify the hypothesis that this point belongs to the obstacle. Furthermore, in order to choose the closest distance to the obstacle the smallest LRF values are examined with the help of a median filter. Such an approach allows to benefit from nice robustness properties, as our avoidance strategy relies on several laser points as opposed to just one as it has been done in all the previous works at hand (Folio and Cadenat, 2005), (Adrien D. Petiteville and Cadenat, 2012).

The resulting point will be kept as the SCP for as long as the robot is in a safe distance to the target. Should it however, get too close to the obstacle, the SCP will be recomputed with the newly collected LRF data.

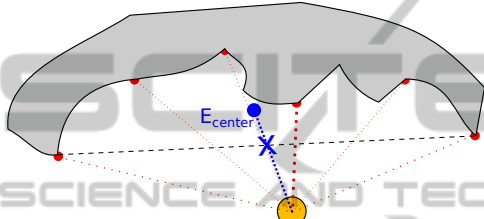


Figure 3: Concept of estimating the Spiral Center Point.

3.2.2 Spiral Conventions and Definition

Once point E_{center} has been defined and we attached a frame denoted by $F_E(E_{center}, \vec{x}_E, \vec{y}_E, \vec{z}_E)$ whose axes are chosen to be equal to the ones of the world frame F_w (same orientation) we can start imagining an appropriate OA. In Figure 4 we now present the spiral concept and its conventions. A complete robot has not yet been visualized in order to clarify our conventions in a less overloaded figure.

First, we denote P_{spiral} as one point of the spiral, while T and N represent the tangent on the spiral and the normal vector of it. The green arrow at the far right of the figure indicates the previous heading of the robot

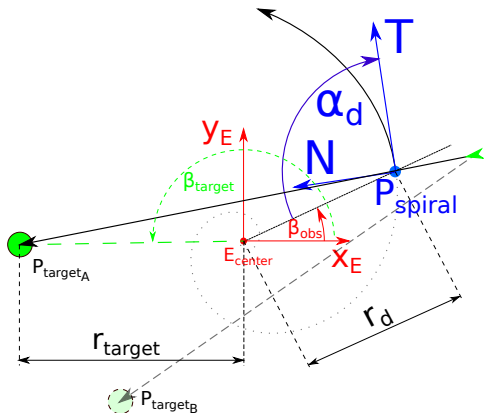


Figure 4: Spiral Conventions.

and will be of importance for the sense of motion which we will discuss later. The spiral we envision is a equiangular spiral and defined by the following polar equation in frame F_E :

$$r_d = r_0 * \exp^{\cot(\alpha_d) * (\beta_{obs_0} - \beta_{obs})} \quad (7)$$

where r_d is the distance between E_{center} and P_{spiral} , β_{obs} represents the angle between x_E and $E_{center} \vec{P}_{spiral}$. Furthermore α_d is defined as the angle from the connecting vector robot-obstacle and the tangent to the spiral. Our convention is that the position of the robot at $t = t_0$, the time when the OA is first triggered, represents the first point of the spiral and will therefore, determine r_0 , β_{obs} and β_{obs_0} . Of those parameters only β_{obs} will vary over time and r_0 and β_{obs_0} will be set to the values of r_d and β_{obs} at $t = t_0$.

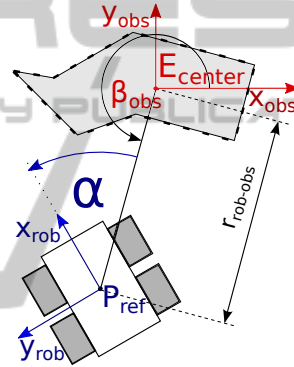


Figure 5: Parameters of the Robot Obstacle Relationship.

Now let us consider Figure 5 where we added a model of the robot. In this figure, we denote $r_{rob-obs}$ as the distance between points E_{center} and P_{ref} and α the angle between \vec{x}_E and $E_{center} \vec{P}_{ref}$. So in the optimal case $r_{rob-obs}$ as well as α should be equal to their counterparts, r_d and α_d .

The equiangular spiral (from Equation 7) is defined by four parameters r_0 , α_d , β_{obs} and β_{obs_0} . So far we managed to set all parameters but one. To properly choose α_d we may consider the following guidelines deduced from (Boyadzhiev, 1999) (review Figure 2 on page 3):

- if $\alpha_d > \frac{\pi}{2}$: an outward spiral is performed and the robot pulls away from the obstacle;
- if $\alpha_d < \frac{\pi}{2}$: an inward spiral is realized and the robot closes the distance towards the obstacle;
- if $\alpha_d = \frac{\pi}{2}$: a circle is obtained and the robot maintains at a constant distance to the obstacle.

While the first and third cases seem to offer attractive motion behaviors, the second one may also be interesting if several obstacles lie in the robot's vicinity

(e.g. a cluttered environment) or if a mobile obstacle is expected to cross the vehicle path. Indeed, the robot will then have the ability to go closer to the obstacle. A nominal value for α_d and its effects on the robot are given in the results section.

3.2.3 Sense of Motion Around the Obstacle

One final detail we have not mentioned so far concerns the sense of motion around the obstacle. In Figure 4 we have hinted on this "orientation" of the spiral which is dependent on the position of the target (P_{target_A} or P_{target_B}) towards the robot and the obstacle. In fact, when choosing our spiraling parameters we have to decide on the orientation before. Taking a look back onto the figure the robot has two options. Either it moves clockwise, cw (e.g.: when P_{target_B} is the target), or counter-clockwise, ccw (e.g.: when P_{target_A} is the target), around the obstacle. For now there is only one condition which dictates our spiral orientation will be the location of the target in relation to the robot reference (P_{ref}) and the obstacle reference point (E_{center}). P_{target_B} , the green point with an interrupted enclosing line displays a target which would lead to a change in the spirals orientation to a clockwise manner. For the situation mentioned before, where it would be necessary to recompute the spiraling center point, we will keep the orientation to avoid being trapped by the obstacle.

3.3 The Obstacle Avoidance Control Law

3.3.1 Control of the Mobile Base

The intention of the following paragraph is to find a control law which can be sent to the robot to make it move according to the spiraling concepts presented before. This control law was deduced from the analysis of the expected motion of the robot. First of all, we have decided to impose a constant (non-zero) linear velocity denoted by v_0 .

After that our approach for the control law is to firstly, minimize the error between the desired angle (α_d) and the current angle of the robot towards the obstacle (α) and secondly, to make the distance $r_{rob-obs}$ converge towards r_d given by Equation 7. The first assignment is achieved by the first addend of ω (e_{α_d}) in the manner of a task function approach as it is used throughout this paper (VS-controller and control of the camera platform later on). Furthermore a parameter χ is introduced which is dependent on the current distance between the obstacle and the robot, measured constantly with the help of the LRF. Hence, χ will enable us to

address our second assignment for this control law. Also, it resembles a precautionary measure which is taken to ensure that the robot stays on the path we envisioned and can never enter into dangerous areas which in turn ensures a much smoother movement of the robot. Since we have chosen to set the robot's linear speed to a non-zero constant value v_0 the angular speed is the sole control input upon which we act to guarantee the collision free navigation.

$$\omega = \begin{cases} e_{\alpha_d} + \chi(r_d), & \text{if ccw} \\ -e_{\alpha_d} + \chi(r_d), & \text{if cw} \end{cases} \quad (8)$$

$$e_{\alpha_d} = \alpha - \alpha_d \quad (9)$$

Here χ is given in another task function approach:

$$\chi = \begin{cases} e_{r_d} * \lambda_r, & \text{if ccw} \\ -e_{r_d} * \lambda_r, & \text{if cw} \end{cases} \quad (10)$$

$$e_{r_d} = r_{rob-obs} - r_d \quad (11)$$

where λ_r is a positive gain and adjusts between our angle and distance needs. We can furthermore observe that Equation 8 and Equation 10 are equipped to deal with either a cw or a ccw motion around the obstacle. Equation 8 can be applied as long as the sampling rate is sufficiently high and the differences in the velocity of the robot and the obstacle do not exceed certain limits. Upon reaching those limits it is still possible to compensate with the λ_r . However, in all simulations those limits were never reached.

3.3.2 Control of the Pan-Tilt-Unit

Following our previous paragraph, the mobile base is controlled using the following velocities:

$$\dot{q}_{base} = \begin{bmatrix} v_0 \\ \omega \end{bmatrix} \quad (12)$$

where ω is given by Equation 8. This control law ensures the non-collision. However, it is also necessary to control the PTU, or simply pan-platform, of the camera system so that the visual features are never lost. This is a mandatory condition which insures that it will be possible to switch back to VS, once the obstacle will not be inducing any danger. Furthermore, the continuous computation of VS is necessary for the execution of the guarding conditions as we will see soon. To do so, we propose to regulate the following error to zero:

$$e_{pan} = Y - Y_d \quad (13)$$

where Y and Y_d corresponds to the current and desired ordinate of the center of gravity of the target in the image. Separating the terms related to the pan-platform

and to the mobile base in the robot’s Jacobian leads to:

$$T_c = [J_b \ J_{pan}] \dot{q} \quad (14)$$

Now introducing the interaction matrix L_y corresponding to the ordinate Y of a point, we may deduce that:

$$\dot{Y} = L_y T_c = L_y J_b \dot{q}_{base} + L_y J_{pan} \omega_{cam} \quad (15)$$

A controller making e_{pan} exponentially decrease to zero is given by:

$$\omega_{cam} = -\frac{1}{L_y J_{pan}} (\lambda_{pan} e_{pan}) + L_y J_b \dot{q}_{base} \quad (16)$$

where λ_{pan} is a positive scalar.

3.4 The Supervisor and its Guarding Conditions

The supervisor is the high-level-controller which is able to choose from a list of controllers, such as VS or OA, the most suitable controller for the situation at hand. In Figure 6 a schematic can be found which explains how the supervisor is using guard conditions to evaluate which controller is to be chosen. The ellipses in this figure represent these different controllers and the arrows visualize the possible switching directions. A controller we have not talked about so far is the "Trajectory based Navigation". In cases where no visual clues can be detected to guide the robot the supervisor will switch to this controller to compute the robot’s motion. The method used to do so is presented in (Marder-Eppstein et al., 2010) and was implemented in the Robot Operating System (ROS) Navigation Stack. It relies on a constantly updated metric map to guide the robot.

Guarding conditions, or simply guards, are methods which tell the supervisor to switch behavior. Our guard for switching to OA is very basic. Whenever the LRF detects points which are closer than the trigger distance ($r_{OA-trigger}$), the supervisor will switch to OA behavior. To disengage the OA when the obstacle is passed we keep computing the VS controller without applying its computed velocities to the robot (Petiteville and Cadenat, 2014). Furthermore, we estimate the pose of the robot if we would apply these

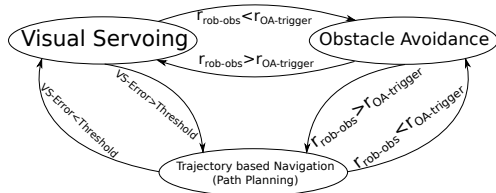


Figure 6: Schematic of the Supervisor.

commands. This assessment is achieved with a simple Euler Scheme (discretization) meaning we will compute the next position of the robot by using its current position and adding the derivative of the current velocity. If the algorithm realizes that using the VS-Controller will actually move the robot further away from the obstacle, a guarding condition will instruct the supervisor to switch back to VS. In order to not constantly switch behaviors this situation needs to be observed a certain number of times successively.

4 SIMULATION AND RESULTS

4.1 Simulation Environment

The Air-Cobot-Robot will be using ROS. Since the recommended simulator for ROS is Gazebo we chose this simulator as our test environment. However, in order to visualize our findings we figured that neither ROS, Gazebo or even RVIZ can provide a sufficient presentation of our findings in just a few images. Thus, in order to present our simulation results we used the ROS recording tool (ROS-bag) and a ground truth Gazebo plug-in to capture the robot and obstacle positions and orientation. Those recordings are then read into Matlab and plotted as trajectories in a 2D-plot. At "http://homepages.laas.fr/mfutterl/" we provide a recording (video file) of the second experiment.

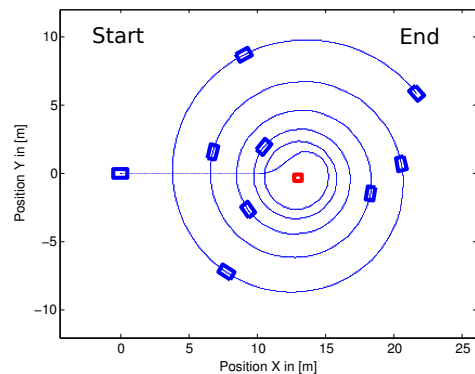


Figure 7: Proof of Concept of an outwards spiraling Obstacle Avoidance.

Figure 7 displays one of those recordings. Here we present our capability of spiraling around an obstacle by applying Equations 8, 10 and 7 with an $\alpha_d > 90^\circ$. The figure displays successive poses of a robot (blue rectangles) going from left to right (blue path) and also the static obstacle (red rectangle). As we can see, the obstacle is successfully avoided by the robot executing a spiral motion around it, as expected. Further-

more, one can observe that the performed spiral is an outward spiral due to the chosen α_d .

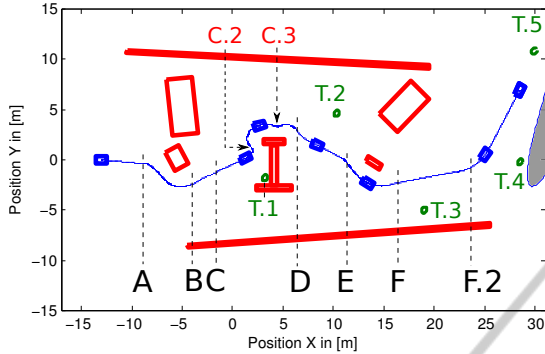


Figure 8: Simple Avoidance Experiment for static Obstacles.

In Figure 8 we present a scenario where the OA controller is coupled with a VS controller. The simulation environment is set up with the projects requirements in mind (provided video file). Mainly the approach towards an aircraft (grey area on the far right side of the figure) is simulated as well as reaching the first checkpoint at its jet engine. All the obstacles (red rectangles) are static and non-occluding and the distance at which the OA is triggered is set to 2.5 meters. Furthermore, we have implemented a very basic topological map allowing the robot to advance to the next visual marker (T.1-T.5) whenever the VS error is sufficiently low. Instead of spiraling around the obstacle indefinitely, a guard enables the robot to leave the OA controller when a safe passage towards the current landmark is possible. By taking a closer look, we can observe the VS behavior from Start to A, shortly from B to C, from D to E and finally from F through F.2 to the final position. The spiral obstacle avoidance is used from A to B (counter-clockwise), from C to D (cw) and from E to F (ccw) with an α_d of $\frac{\pi}{2}$. Especially the second obstacle is interesting as it offers the robot a convenient trap forcing it to recomputing the spiral center point two times during its avoidance (C.2 and C.3). For the other two obstacles, the recomputation of the SCP is not necessary. By consulting the results of this experiment we can conclude that our approach is applicable and works as expected.

In Figure 9.top the linear velocity for the previous experiment is presented. As before, the data is obtained with the help of a Gazebo ground truth plug-in. We can clearly see the time intervals in which the robot was using the VS controller ($\simeq 1.8 \frac{m}{s}$) and the OA controller ($\simeq 0.4 \frac{m}{s}$). The slight "up and downs" during the respective phases are due to the skid steering drive controller and are matter of optimization at the moment. The kinematic model of the robot forces it to

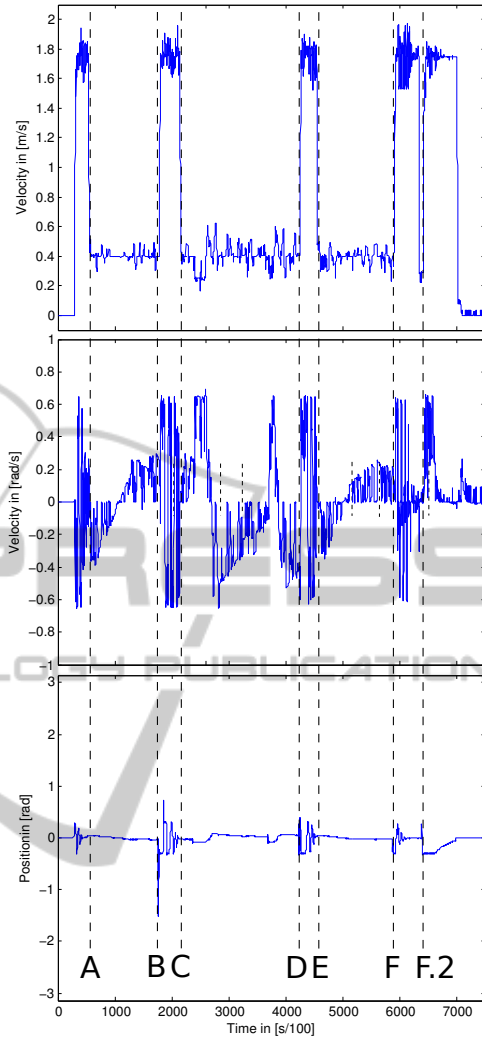


Figure 9: Robot's linear and angular Velocities and Camera Angle.

slow down in order to apply higher changes in angular velocity. A better prediction of the obstacles shape could make these higher angular changes irrelevant in the future, thus, smoothing the robot's trajectory. Figure 9.middle and .bottom give a view on the robot's angular velocity and the camera angle during the mission.

5 CONCLUSION

In this article we have shown that it is possible to use the concepts found in (Boyadzhiev, 1999) and apply them to the OA of a mobile robot. Furthermore, we have succeeded in combining these techniques into a navigational framework including a supervisor and a VS controller. There are still some challenges which

we have yet to conquer such as improving the techniques to choose the center point of the Spiral (SCP) from point-cloud data provided by the LRF. A more sophisticated method to determine this point could be found in either least square methods (also including a window approach to remove points that are too old or are conceivable) or even in matching the acquired points to a predefined simple shape (ellipse, circle, rectangle, etc.). At the moment we are working on applying the algorithms shown in this paper onto moving obstacles and also increasing the robustness of Equation 10 for those situations. Finally, as has been hinted on before, smoothing the robot's velocity controllers is another subject we are currently working on. For the future, we also plan to integrate presented concepts on the real Air-Cobot-Robot and perform tests in a real life situation.

REFERENCES

- Adrien D. Petiteville, A. D. and Cadenat, V. (2012). From the general navigation problem to its image based solutions. *Workshop Vicomor. IROS 12. Portugal*.
- Boyadzhiev, K. N. (1999). Spirals and conchospirals in the flight of insects. *The College Mathematics Journal*, 30(1):pp. 23–31.
- Campion, G., Bastin, G., and Dandrea-Novet, B. (1996). Structural properties and classification of kinematic and dynamic models of wheeled mobile robots. *Robotics and Automation, IEEE Transactions on*, 12(1):47–62.
- Chaumette, F. and Hutchinson, S. (2006). Visual servo control. i. basic approaches. *Robotics Automation Magazine, IEEE*, 13(4):82–90.
- Cherubini, A., Grechanichenko, B., Spindler, F., and Chaumette, F. (2013). Avoiding moving obstacles during visual navigation. In *Robotics and Automation (ICRA), 2013 IEEE International Conference on*, pages 3069–3074.
- Cherubini, A., Spindler, F., and Chaumette, F. (2012). A new tentacles-based technique for avoiding obstacles during visual navigation. In *Robotics and Automation (ICRA), 2012 IEEE International Conference on*, pages 4850–4855.
- Damas, B. and Santos-Victor, J. (2009). Avoiding moving obstacles: the forbidden velocity map. In *Intelligent Robots and Systems, 2009. IROS 2009. IEEE/RSJ International Conference on*, pages 4393–4398.
- Folio, D. and Cadenat, V. (2005). A controller to avoid both occlusions and obstacles during a vision-based navigation task in a cluttered environment. In *Decision and Control, 2005 and 2005 European Control Conference. CDC-ECC*, pages 3898–3903.
- Khatib, M. and Chatila, R. (1995). An extended potential field approach for mobile robot sensor-based motions. In Press, I., editor, *Intelligent Autonomous Systems (IAS)*, pages 490–496, Karlsruhe, Germany.
- Koenig, S. and Likhachev, M. (2005). Fast replanning for navigation in unknown terrain. *Robotics, IEEE Transactions on*, 21(3):354–363.
- Lamiroux, F., Bonnafous, D., and Lefebvre, O. (2004). Reactive path deformation for nonholonomic mobile robots. *Robotics, IEEE Transactions on*, 20(6):967–977.
- Marder-Eppstein, E., Berger, E., Foote, T., Gerkey, B., and Konolige, K. (2010). The office marathon: Robust navigation in an indoor office environment. In *Robotics and Automation (ICRA), 2010 IEEE International Conference on*, pages 300–307.
- Matsumoto, Y., Inaba, M., and Inoue, H. (1996). Visual navigation using view-sequenced route representation. In *Robotics and Automation, 1996. Proceedings., 1996 IEEE International Conference on*, volume 1, pages 83–88 vol.1.
- Mcfadyen, A., Corke, P., and Mejias, L. (2012a). Rotorcraft collision avoidance using spherical image-based visual servoing and single point features. In *Intelligent Robots and Systems (IROS), 2012 IEEE/RSJ International Conference on*, pages 1199–1205.
- Mcfadyen, A., Mejias, L., and Corke, P. (2012b). Visual servoing approach to collision avoidance for aircraft. In *28th Congress of the International Council of the Aeronautical Sciences 2012*, Brisbane Convention & Exhibition Centre, Brisbane, QLD.
- Owen, E. and Montano, L. (2005). Motion planning in dynamic environments using the velocity space. In *Intelligent Robots and Systems, 2005. (IROS 2005). 2005 IEEE/RSJ International Conference on*, pages 2833–2838.
- Petiteville, A. D. and Cadenat, V. (2014). An anticipative reactive control strategy to deal with unforeseen obstacles during a multi-sensor-based. *ECC*.
- Pissard-Gibollet, R. and Rives, P. (1995). Applying visual servoing techniques to control a mobile hand-eye system. In *Robotics and Automation, 1995. Proceedings., 1995 IEEE International Conference on*, volume 1, pages 166–171 vol.1.
- Samson, C., Espiau, B., and Borgne, M. L. (1991). *Robot Control: The Task Function Approach*. Oxford University Press.
- Ulrich, I. and Borenstein, J. (2000). Vfh*: local obstacle avoidance with look-ahead verification. In *Robotics and Automation, 2000. Proceedings. ICRA '00. IEEE International Conference on*, volume 3, pages 2505–2511 vol.3.
- Vilca, J., Adouane, L., and Mezouar, Y. (2013). Reactive navigation of a mobile robot using elliptic trajectories and effective online obstacle detection. *Gyroscope and Navigation*, 4(1):14–25.